Molecular Therapy
Methods & Clinical Development
Original Article

Probing aspects of extracellular vesicle associated AAV allows increased vector yield and insight into its transduction and immune-evasive properties

Ming Cheng,[1,2,3,7] Demitri de la Cruz,[1,2,3,7] Adam V. Crain,[1,2,3] Paula Espinoza,[1,2,3] Carrie Ng,[1,2,3] Zachary C. Elmore,[4] Aravind Asokan,[4,5,6] and Casey A. Maguire[1,2,3]

[1]Department of Neurology, Massachusetts General Hospital, Boston, MA 02114, USA; [2]Molecular Neurogenetics Unit, Massachusetts General Hospital, Charlestown, MA 02129, USA; [3]Harvard Medical School, Boston, MA 02115, USA; [4]Department of Surgery, Duke University School of Medicine, Durham, NC 27710, USA; [5]Department of Molecular Genetics & Microbiology, Duke University School of Medicine, Durham, NC 27710, USA; [6]Department of Biomedical Engineering, Duke University, Durham, NC 27710, USA

Extracellular vesicle-associated adeno-associated virus vectors (EV-AAVs) are generated during production in 293 cells. EV-AAV provides desirable gene delivery traits such as greater resistance to antibody neutralization and increased transduction of organs *in vivo* compared with conventional AAV. Despite these promising data, better characterization of EV-AAV is needed. We used density gradient ultracentrifugation to separate EV-AAV from free AAV to determine the yields and functional activity of EV-AAV. We found that the fraction of EV-AAV to conventional AAV in culture media from six AAV serotypes ranged from 0.5% to 12%. Next, we assessed whether intraluminal EV-AAV9 could mediate functional transduction of cells and observed that a portion of EV-AAV9 are intraluminal and mediated transduction of cultured cells *in vitro* and *in vivo* and evade antibodies compared with conventional AAV9. We tested whether *trans*-expression of membrane-associated accessory protein (MAAP) from AAV8 (MAAP8) or AAV9 (MAAP9) with AAV9 Cap/AAV9 MAAP null would alter yields of EV-AAV9. *Trans*-expression of MAAP8 or MAAP9 increased yields of EV-AAV9 compared with the *cis*-expression of AAV9 Cap/AAV9 MAAP. Finally, we found that the capsid was required for efficient transduction of cultured cells by EV-AAV. In sum, these data provide a foundation for the development of EV-AAV vectors.

INTRODUCTION

Adeno-associated virus (AAV) vectors can mediate efficient *in vivo* delivery, providing therapeutic levels of transgene expression; this efficiency has led to the approval of several AAV-based medicines in the United States and Europe.[1] The structural proteins of AAV, VP1, 2, and 3, form the virus capsid which is responsible for all of steps necessary for transduction including cell surface binding, internalization, intracellular trafficking, and even recruitment of transcriptional machinery.[2,3] The capsid is also a target for the host's immune response, which can block therapeutic efficacy,[4,5] and in some cases lead to serious adverse events[6] and even patient death.[7–10] Strategies to mitigate the immune response to AAV is an intense area of investigation. One strategy to reduce immune recognition of the AAV capsid is to shield it in a manner that immune components such as humoral immunity (antibodies) or complement cannot readily access. More than a decade ago, we observed that AAV capsids are present on the surface and interior (lumen) of extracellular vesicles (EVs).[11] Since then, our group and several others have demonstrated that EV-AAV displays several properties such as increased antibody evasion and transduction of target cells *in vivo* compared with conventional (non-enveloped) AAV vectors.[11–19] Since EV-AAV is a relatively nascent technology, there are several mechanistic questions as well as areas of improvement needed. Areas of improvement center around the yield of EV-AAV compared with conventional (non-enveloped) AAV. Mechanistic studies are needed to address unknowns such as whether intraluminal AAV capsids in EV-AAV are capable of transducing cells, which would have important implications for the development of the system. Additionally, whether the AAV capsid is an essential component of EV-AAV needs to be determined, as this could drive the development of the system in a different direction.

In this study, we used an optimized density gradient ultracentrifugation protocol to highly separate EV-AAV from AAV, which allowed us to design experiments to specifically probe the characteristics and functions of EV-AAV.

RESULTS

Isopycnic gradient purification of AAV from the media facilitates quantitation of EV-AAV

Our group[13] and others[20] have used iodixanol density gradient ultracentrifugation to estimate the percentage of EV-AAV9 and EV-AAV1 in the media, which was approximately 10% and approximately 25%,

Received 1 April 2024; accepted 14 January 2025;
https://doi.org/10.1016/j.omtm.2025.101407.

[7]These authors contributed equally

Correspondence: Casey A. Maguire, Department of Neurology, Massachusetts General Hospital, Boston, MA 02114, USA.
E-mail: cmaguire@mgh.harvard.edu

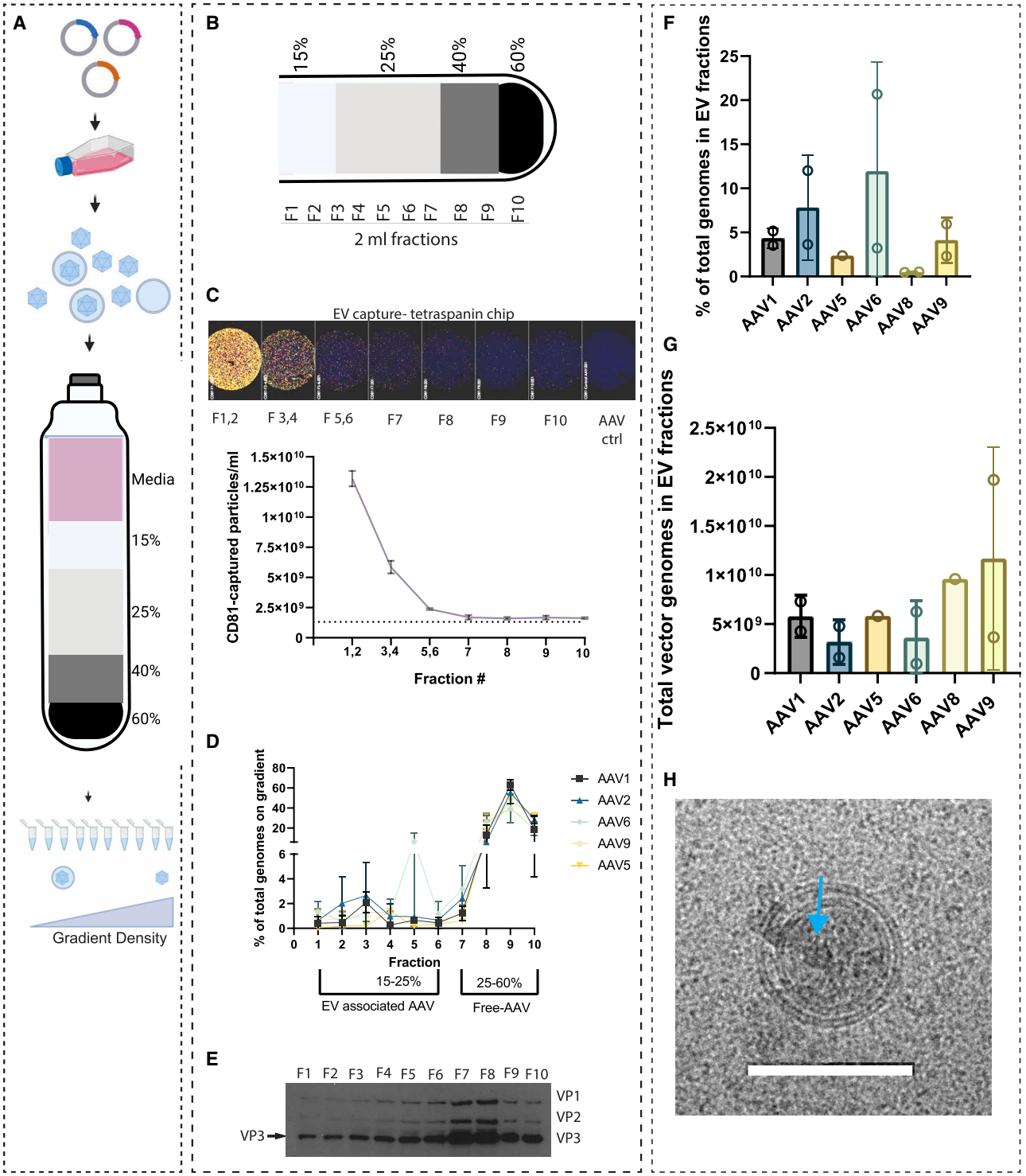

Figure 1. Characterization and quantitation of EV-AAV in producer cell media using iodixanol density gradient ultracentrifugation

(A and B) Overview. 293T cells are transfected with AAV plasmids to generate the AAV serotype of choice (AAV1, AAV2, AAV5, AAV6, AAV8, and AAV9). At a given time point, media is isolated and a density gradient ultracentrifugation performed. The gradient is fractioned and EV-AAV are predicted to be in the less dense fractions and free AAV in denser fractions. (C) Quantitation of tetraspanin positive EVs using the ExoView instrument. High concentrations of EVs are in less dense fractions. (D) Quantitation of AAV vector genomes (vg) on gradient (note y axis scale break). (E) VP1,VP2, and VP3 AAV6 capsid immunoblot. Arrow points to VP3 band detected in all fractions. F7 and F8 are

(legend continued on next page)

respectively. Both of these studies used a tedious and lengthy (18 h centrifugation) multi- 11- to 14-layer gradient. Recently another group used a simpler four step iodixanol gradient with a shorter (3 h centrifugation) to isolate EV-AAV.[21] We tested this gradient to separate EV-AAV from naked AAV capsids from media of producer cells harvested in the 24 h window between 48 and 72 h after transfection (Figure 1A). We tested this for AAV1, AAV2, AAV5, AAV6, and AAV9 to observe serotype specific differences. Gradients were fractioned in 2 mL aliquots (Figure 1B) and assayed by qPCR for AAV genomes, ExoView technology for EV quantitation, and western blot to detect AAV capsid proteins (VP1, VP2, and VP3). ExoView combines an ELISA-like protocol to capture EVs using an antibody, in this case an anti-tetraspanin (CD81) antibody, with fluorescence and interferometric microscopy to count EVs. We have previously shown that EV-AAV from 293T cells have high levels of CD81 on their surface.[12] Dilutions of each fraction were performed and incubated with the anti-CD81 coated chips. We also incubated chips with purified conventional AAV to determine background and non-specific binding to AAV, which could confound the results. Detection antibodies against CD81, CD63, and CD9 allow detection of EVs with these tetraspanins. We found that the CD9 antibody had some increase in detecting the control AAV sample over a blank chip, so we excluded CD9 counts in our analysis and focused on CD81 and CD63. Direct imaging of the chips showed high levels of CD81-captured EVs in early, less dense fractions of the gradient as expected, with a large drop off after pooled fractions 3 and 4 (Figure 1C). Next, we quantitated the AAV vector genomes (vg) in each fraction. For all serotypes, the majority of vg (approximately 90%) were in the dense fractions 8–10, which are likely free, non-enveloped AAV (Figure 1D). Detection of vg in fractions 1–4 (putative EV fractions) was also detected for all serotypes (Figure 1D). A peak in fraction 5 was observed in one of two preps of AAV6, which may have been caused by some mixing of the gradient regions while fractioning the gradient. We detected capsid proteins with a commercially available antibody to VP1-3. As expected from the vg data, fractions 8–10 had readily detectable levels of VP1, VP2, and VP3 (Figure 1E). Similarly, VP1, VP2, and VP3 were observed in fractions 1–6 (Figure 1E). Fractions 7 and 8 had the highest levels of VP proteins, even though fraction 7 had low numbers of vg. Fractions 7 and 8 are at the 25%/40% iodixanol interface, which contains less-dense, empty capsids, so this likely reflects an area of the gradient with empty capsids (F7) and mixture of full and empty capsids (F7 and F8). Based on the ExoView, vector genome, and capsid immunoblot data, we chose fractions 1–6 as putative EV-AAV fractions and F7–F10 as free AAV fractions. We especially wanted to avoid F7 in our EV-AAV preps, as we do not want free AAV capsids in our product, which could confound transduction and neutralization assays. Using the F1–F6 vg data, we quantitated the percentage of AAV genomes on the gradient in the EV-AAV fraction. We also included AAV8 in this quantitation. The average EV-AAV percentage ranged from 0.5% (AAV8) to 11.95% (AAV6), (not significant by ANOVA) (Figure 1F). Total vector genomes in the EV-AAV fractions for each serotype ranged from 3.18×10^9 vg (AAV2) to 2×10^{10} vg (AAV9) (not significant by ANOVA) (Figure 1G). The percentage for EV-AAV9 was similar to those reported with the 11-step iodixanol gradient.[13] Comparing yields in the putative EV-AAV vs. conventional AAV fractions is shown in Figure S1. Fold differences in yields between the conventional AAV fractions vs. EV-AAV fractions ranged from 3.7-fold (AAV6) to 200-fold (AAV8) (Figure S1).

To visually assess the composition of the putative EV-AAV fraction, we subjected pooled fractions 1–6 to cryogenic electron microscopy (Cryo-EM). As expected from prior Cryo-EM analysis of EVs, we observed many spherical vesicles of varying sizes in the preparation, including uni- and multi-lamellar structures (Figure S2). We were also able to detect AAV capsids within some of the EVs (Figure 1H).

Intraluminal EV-AAV9 is capable of transduction and resistance to neutralizing antibodies

By Cryo-EM, we have observed free AAV capsids and AAV capsids bound to the surface as well as on the interior (lumen) of EVs.[11,14,16] Understanding whether intraluminal EV-AAV is capable of transduction and antibody resistance is a remaining question. We reasoned that isolating EV-AAV on the iodixanol gradient would remove the majority of free AAV capsids and that further removal of EV-bound AAV capsids using an anti-AAV9 antibody would allow us to assess transduction and antibody neutralization. First, we produced AAV9 encoding firefly luciferase (FLuc) under a CAG expression cassette (AAV-CAG-FLuc). Next, we harvested media and purified EV-AAV9-FLuc in fractions 1–6 from the iodixanol gradient. We kept one aliquot of the preparation as EV-AAV9-FLuc that contained both intraluminal and surface-bound EV-AAV. Another aliquot of the purified sample was incubated with streptavidin-conjugated magnetic beads (control beads). The final aliquot of purified AAV was incubated with anti-AAV9 antibody-bound streptavidin beads (Figure 2A). We first tested the efficiency of anti-AAV9 bead pulldown and found it removed 99.8% of conventional AAV9 capsids (only 0.34% of AAV was pulldown resistant) (Figure 2B). With the pulldown efficiency confirmed, we tested resistance of EV-AAV9 to anti-AAV9 pulldown compared with control beads (i.e., no anti-AAV9 antibody was bound to the beads). We normalized the anti-AAV9 bead sample to the control bead sample. This calculation demonstrated that 11.3% of AAV genomes were resistant when incubated with anti-AAV9 beads (Figure 2B). This indicates the existence of a sizable fraction of EV-AAV that has no surface AAV and only luminal AAV. We also compared the pulldown resistance of gradient-purified AAV1, AAV2, and AAV6 to their corresponding

putative empty capsid fractions. (F) Percent of vg on gradient in EV-AAV fractions 1–6. (G) Total vg on gradient in EV-AAV fractions 1–6. Error bars in all panels are the standard error from the mean. Two gradients per serotype were run, except for AAV5 which was performed once. Each data point in (F) and (G) represents an independent purification of the respective serotype of AAV. Two purifications were performed each for AAV1, AAV2, AAV6, and AAV9. AAV5 and AAV8 were purified once. An ordinary one-way ANOVA was not significant for either (F) or (G). (H) Cryo-EM image showing a double-layered EV containing an AAV capsid (blue arrow). Scale bar, 100 nm.

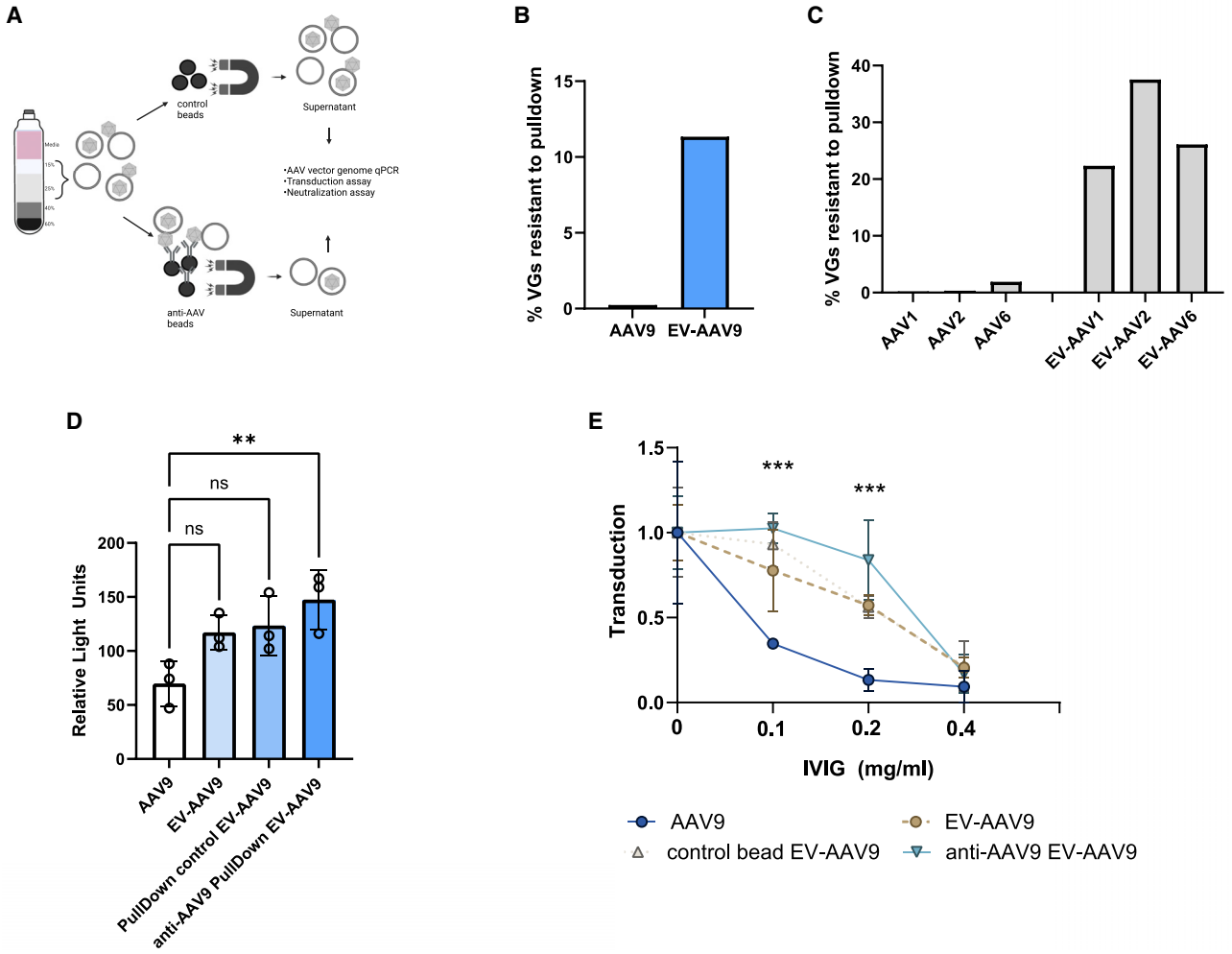

Figure 2. A substantial portion of AAV capsids and genomes in EV-AAV preparations are intraluminal and mediate transduction of cells and resistance to antibody neutralization

(A) EV-AAV is purified from media and then extra-luminal AAV capsids are removed with anti-AAV9 conjugated beads. (B) Purified AAV9 or EV-AAV9 were incubated with control beads or anti-AAV9 conjugated beads. (C) Purified AAV1, AAV2, AAV6, or their cognate EV-AAV preparations were incubated with control or anti-AAV conjugated beads (AAVX antibody). In (B) and (C), the percent resistance to pulldown in the EV-AAV fraction is putative intraluminal AAV. (D) Transduction of HeLa cells with intraluminal EV-AAV9. (E) Intraluminal AAV resists neutralization to IVIg compared with AAV9.

ns, not significant; $^{**}p = 0.009$; $^{***}p < 0.001$.

EV counterparts using AAV-X biotinylated antibody, which can bind many different serotypes.[22] For standard AAVs, only 0.22% to 1.89% of AAV was resistant to anti-AAVX pulldown when normalized to the beads-only control sample (Figure 2C). However, VGs in EV-AAV were more resistant to pulldown with AAV-X, ranging from 22.3% to 37.5% (Figure 2C). To understand if AAV9 vectors solely inside EVs could mediate transduction of cultured cells, we transduced HeLa cells with equal doses (10^4 vg/cell) of conventional AAV9, EV-AAV9, control bead incubated EV-AAV9, and anti-AAV9 pulldown-resistant EV-AAV9 (i.e., intraluminal AAV9). Interestingly all groups trended toward greater transduction efficiency over AAV9, although only the intraluminal EV-AAV9 group's increase was statistically significant ($p = 0.009$) (Figure 2D). We next compared each group's resistance to transduction neutralization by serial 2-fold dilutions of intravenous immunoglobulin (IVIg). As expected, AAV9 was efficiently neutralized at all dilutions of IVIg. As expected from prior reports, EV-AAV9 had higher resistance to antibody neutralization at 1:1,000 and 1:500 IVIg dilutions. Intraluminal EV-AAV9 showed statistically significant enhanced resistance to both 1:1,000 and 1:500 dilutions of IVIg. All groups were efficiently neutralized at the highest concentration of IVIg (1:250 dilution) (Figure 2E).

In vivo injection of AAV9, EV-AAV9, and intraluminal EV-AAV9-GFP

To test whether intraluminal EV-AAV9-GFP could mediate functional transduction *in vivo*, we injected adult C57BL/6 mice into

the striatum with 1.27×10^7 vg each of AAV9-CAG-GFP, EV-AAV9-CAG-GFP, or intraluminal EV-AAV9-CAG-GFP. Four weeks after injection, mice were euthanized and brains harvested for cryosectioning and immunofluorescence microscopy (Figure 3A). We examined anti-GFP immunostained sections spanning the injection site for transduced cells, and observed transduction for all groups in all mice, including intraluminal EV-AAV9 (Figure 3B). Although there was some inter-animal variability, likely owing to the very low dose used, the most remarkable transduction was observed for the EV-AAV9 group, which displayed an intense area of transduced cells in two of the three injected mice, (Figures 3B and 3C). Quantitation of the transduced area of the injection site revealed similar values for AAV9 and intraluminal AAV9, while EV-AAV9 was 3.4-fold higher, although this difference did not attain statistical significance (Figure 3D). We also stained sections with antibodies to NeuN and GFAP to detect transduction of neurons and astrocytes, respectively, in each group. We observed that all groups transduced neurons (Figures 3E and S3). We also readily observed astrocyte transduction in the AAV9 and EV-AAV9 groups (Figure S4). Interestingly, GFAP staining qualitatively seemed to be less pronounced for the intraluminal EV-AAV9 group (Figure S4).

Trans-expression of AAV8 or AAV9 MAAP increases yields of EV-AAV9

Recently it was discovered AAV encodes a so-called membrane-associated accessory protein (MAAP),[23] and that MAAP is involved in AAV vector egress from producer cells.[24] Heterologous expression of MAAP from AAV8 (MAAP8) during production of AAV9 without endogenous MAAP (AAV9 MAAP null) increased the percentage of AAV9 genomes in the media, even greater than AAV9 with endogenous MAAP9.[24] While these experiments showed that AAV9 yields in media could be increased with MAAP8 overexpression, they did not define whether the released AAV vectors were free capsids or associated with EVs. Here, we explored whether *trans*-expression of MAAP8, could be used to increase the yield of EV-AAV9. MAAP8 is expressed from a rep/cap plasmid which expresses AAV8 MAAP under the endogenous p40 promoter, but Cap and AAP is not expressed due to site-directed mutagenesis of their respective start codons. We produced AAV in 293T cells and harvested media at day 3 after transduction and fractioned the media into free AAV9 and EV-AAV9 as before. We tested the following groups: AAV9 cap/MAAP9 null, AAV9 cap/MAAP9 null + MAAP8, AAV9 cap/MAAP9, and AAV9 cap/MAAP9 + MAAP8 (Figure 4A). We observed a 5.6-fold increase ($p = 0.0055$) in EV-AAV9 yields when MAAP8 was supplemented in AAV9 MAAP9-null transfected cells (Figure 4B). A 2.3-fold increase (not significant) was observed when MAAP8 was complemented in AAV9 MAAP9-transfected cells (Figure 4B). A 3-fold increase ($p = 0.02$) was observed with AAV9 MAAP-null + MAAP8 compared with AAV9 MAAP9 (Figure 4B). Interestingly, MAAP8 also increased the yield of free AAV (fractions 7–10), with the greatest effect observed in the AAV9 cap/MAAP-null group (Figure 4C). We analyzed the fraction of EV-AAV and free AAV in the different groups. The profile was similar among the different groups (approximately 2% EV-AAV, approximately 98% free AAV) with a very slight increase in the AAV9 MAAP9 + MAAP8 groups (Figure 4D). We next assessed whether MAAP8 could enhance media yields of EV-AAV9 compared with conventional AAV9 cap/MAAP9 production over multiple time points. Cells were transfected with either AAV9 cap/MAAP9 or AAV9 cap/MAAP null + MAAP8, as the latter group gave the highest yield increases in the previous, day 3 experiments. For both groups, the kinetics displayed a similar trend with very low levels of AAV genomes at day 1 with a large increase at day 2, with value peaking at day 3 and showing a decline at day 4 (Figure 4E). MAAP8 trans complementation showed the greatest enhancement at day 3 (1.66-fold; $p < 0.0001$), although a small yet significant increase ($p = 0.0068$) was also observed at day 4 (Figure 4E). We next tested whether expression of MAAP9 in trans in the AAV9 MAAP9-null system could increase yields of EV-AAV9. For this experiment, we used pcDNA plasmids with cytomegalovirus (CMV) promoters driving transcription of either MAAP8 or MAAP9 (Figure S5A). We tested transfection of three separate amounts of pcDNA-MAAP/plate (1, 3, and 10 μg). At the highest amount of plasmid for both pcDNA-MAAP8 or MAAP9, we observed more rounded cells, dimmer expression of the reporter (GFP) plasmid and visibly fewer attached cells at harvest compared with the other groups (data not shown). This suggested that the overexpression of MAAP with the strong CMV promoter caused cellular toxicity. Due to the apparent toxicity, we focused on the two lower concentrations for gradient ultracentrifugation and fraction analysis for AAV genomes. At 1 μg of pcDNA-MAAP8 or MAAP9 plasmids, the EV-AAV and free AAV fractions were higher than AAV9 MAAP9-null alone, but did not increase over AAV9 MAAP in cis (Figure S5B). However, at 3 μg of pcDNA-MAAP9, EV-AAV9 yields were increased by 2-fold over AAV9 in cis and free AAV9 yields by 3.6-fold (Figure S5C). Interestingly, pcDNA-MAAP8 expression in trans with AAV9 MAAP null did not increase yields over AAV9 (Figures S5B and S5C).

Vector genomes packaged inside the AAV capsid is required for robust transgene expression from EV-AAV vectors

For conventional AAV, it is well established that AAV genomes are packaged into the capsid and the capsid is required for all steps leading up to transduction. However, EVs can themselves function as delivery vehicles, so it is plausible that AAV genomes/plasmids could be packaged inside EVs and mediate transgene expression independently of the AAV capsid. To test this possibility, we produced AAV8 vectors with conventional rep/cap plasmids or an AAV8 rep/cap-null plasmid (Figure 5A). Both productions included an AAV-CBA-FLuc transgene expression cassette. We purified EV-AAV from fractions 1–6 of the iodixanol gradient and performed qPCR to determine the yield of either preparation. EV-AAV8 capsid vectors yielded 13.7-fold higher vector genomes than EV-AAV produced without capsid plasmid (Figure 5B). This suggests that the majority of genomes in EV-AAV are packaged inside AAV capsids. Next, we incubated HeLa cells with 6.66×10^3 vg/cell of either EV-AAV8-CBA-FLuc or capsid-less EV-AAV-CBA-FLuc and harvested cells

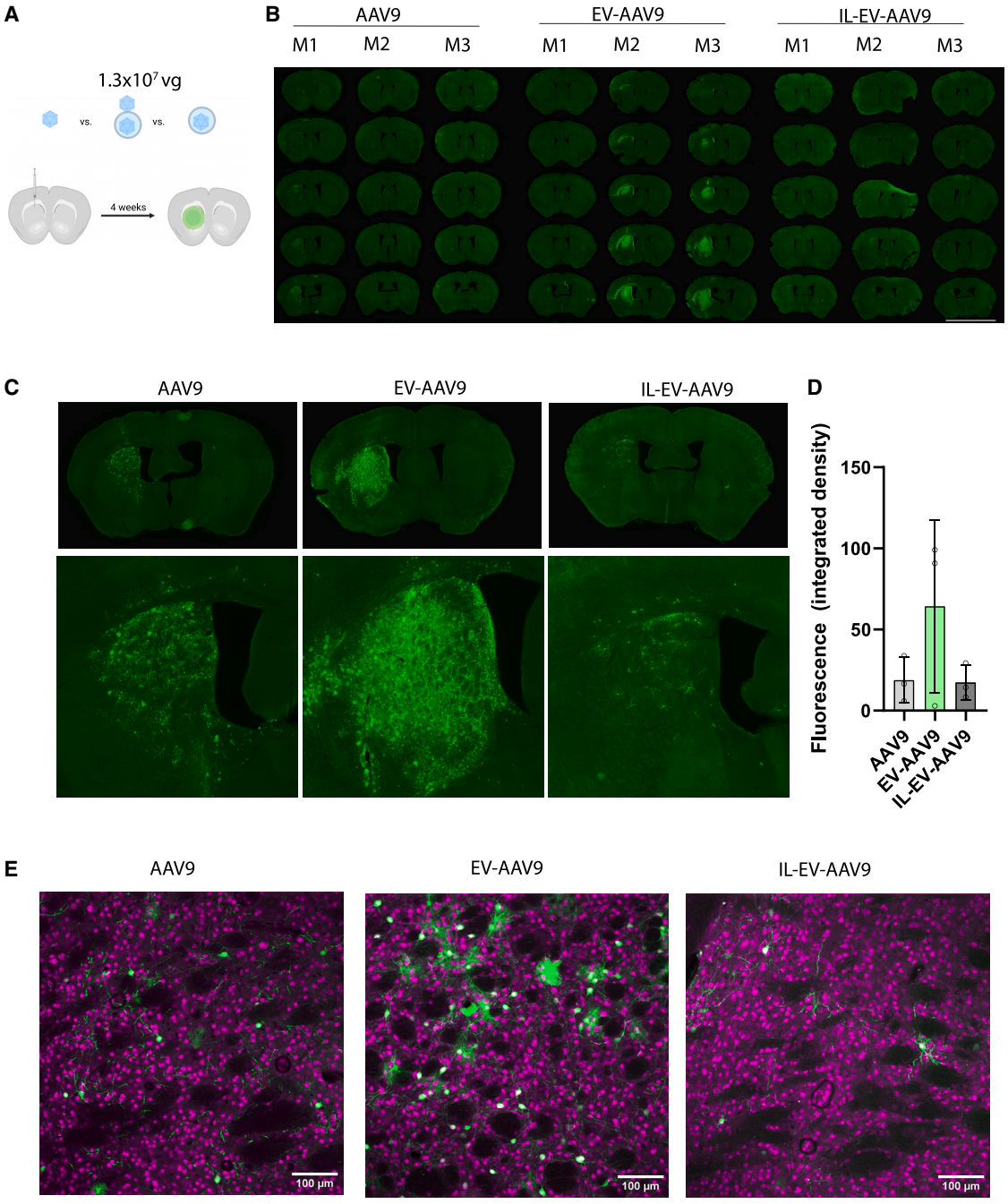

Figure 3. EV-AAV9 and intraluminal EV-AAV9 mediate transduction of neurons after direct low-dose intracranial injection in adult mice

(A) Intracranial injection of C57BL/6 adult mice with AAV9, EV-AAV9, or intraluminal EV-AAV9. All vectors packaged an AAV-CAG-GFP cassette and were injected at 1.27×10^7 vg; $n = 3$ mice/vector group. (B) Whole hemisphere anti-GFP immunostaining for each group. Scale bar, 1 cm. (C) Zoom-in on transduced sections of representative mice from each vector group. (D) Quantitation of transduced area/group. The area of transduction was calculated using integrated density of pixel intensity. (E) Neuronal (NeuN) immunostaining shows colocalized with some of the transduced cells in each vector group. Scale bar, 100 µm.

48 h later. For capsid-less EV-AAV, transduction levels were very low, only approximately 2-fold above background levels of the luciferase assay. We observed a 9-fold higher ($p < 0.0001$) transduction level with EV-AAV8 vs. the capsid-less EV-AAV genomes, highlighting the importance of the capsid for efficient transduction of cells (Figure 5C).

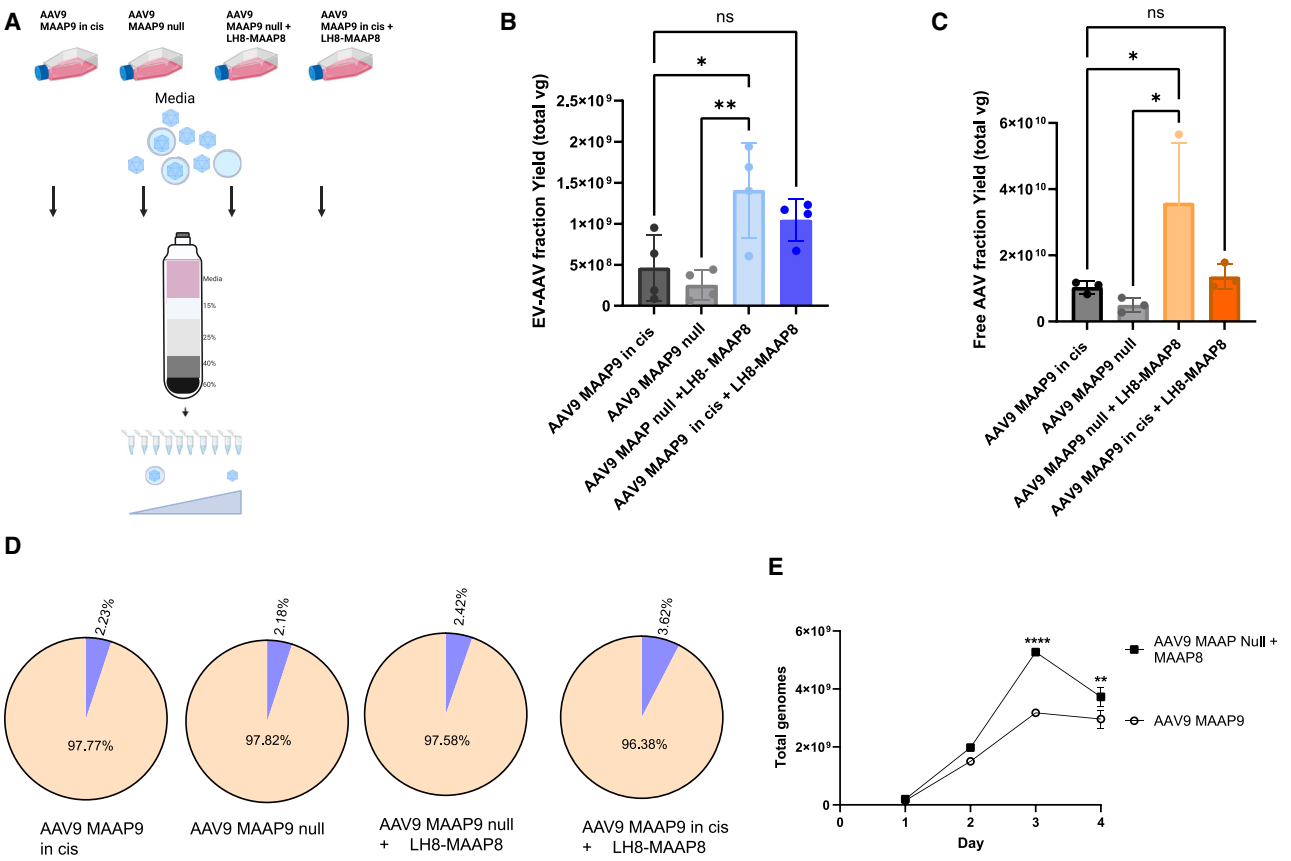

Figure 4. MAAP8 *trans*-complementation enhances both free and EV-AAV9 yields

(A) Experimental overview. AAV9 is produced with (1) AAV9 rep/cap plasmids with a deleted MAAP9 (AAV9 MAAP null), (2) AAV9 MAAP null + MAAP8, (3) AAV9 MAAP9, or (4) AAV9 MAAP9 + MAAP8. Media is harvested, purified on gradients, and EV-AAV and free AAV genomes quantitated by qPCR. (B) Day 3 post-transfection yields of EV-AAV9 genomes in each group. *$p = 0.02$; **$p = 0.0055$; ns, not significant. (C) Day 3 post-transfection yields of free AAV genomes quantitated by qPCR. *$p = 0.042$; **$p = 0.016$. (D) Ratios of EV-AAV to free AAV for each group. (E) Time course of purified EV-AAV9 genomes from cells transfected with AAV9 MAAP9 or AAV9 MAAP null + MAAP8. **$p = 0.0068$; ***$p < 0.0001$. Experiments in (B), (C), and (D) were performed two independent times. Experiment in (E) was performed one time.

DISCUSSION

In this study, we sought to further the understanding of the compositional and functional aspects of EV-AAV. We have previously used sucrose density gradient ultracentrifugation, velocity gradients, differential centrifugation/ultracentrifugation, size exclusion chromatography, and 11-step iodixanol density gradients to characterize EV-AAV.[11–13] While each method has its benefits and drawbacks, density gradient ultracentrifugation remains the gold standard for purity of biomolecules such as viruses and EVs. That said, gradients such as the 11-step iodixanol density gradient we and others have previously used is extremely time consuming and tedious to generate. For this study we used a recently described four-layer iodixanol density gradient that is simpler to generate, and the centrifugation time is considerably shorter.[21]

We first tested the gradient to separate free AAV from EV-AAV and observed a clear separation as observed by distinct peaks in the EV-rich fractions 1–6 from the EV depleted fractions 7–10. Importantly, empty capsids migrated primarily to fractions 7 and 8 area, which allowed us to assess EV-AAV function without confounding effects from empty capsids. Next, we assessed the yield and percentage of EV-AAV for six of the most used AAV serotypes, AAV1, 2, 5, 6, 8, and 9. While previous work has tested one or more of each of these capsids, this is the first study to produce and characterize all of them under the same manufacturing conditions performed within the same laboratory, allowing comparisons. While there were no significant differences in the yields or percentages of EV-AAV among the different serotypes, there were trends. AAV2 and AAV6 trended toward a higher fraction of EV-AAV in the media compared with the other serotypes. AAV8 and AAV9 trended toward higher yields compared with the other serotypes. It was interesting that, among all tested serotypes, AAV6 stood out for having most favorable percentage of EV-AAV vs. free capsids in the media (Figure S1B). In future studies, it will be interesting to attempt to understand if this improved ratio of EV-AAV to free AAV is due to AAV6 MAAP or the capsid or other factors. Luminally localized EV-AAV capsids

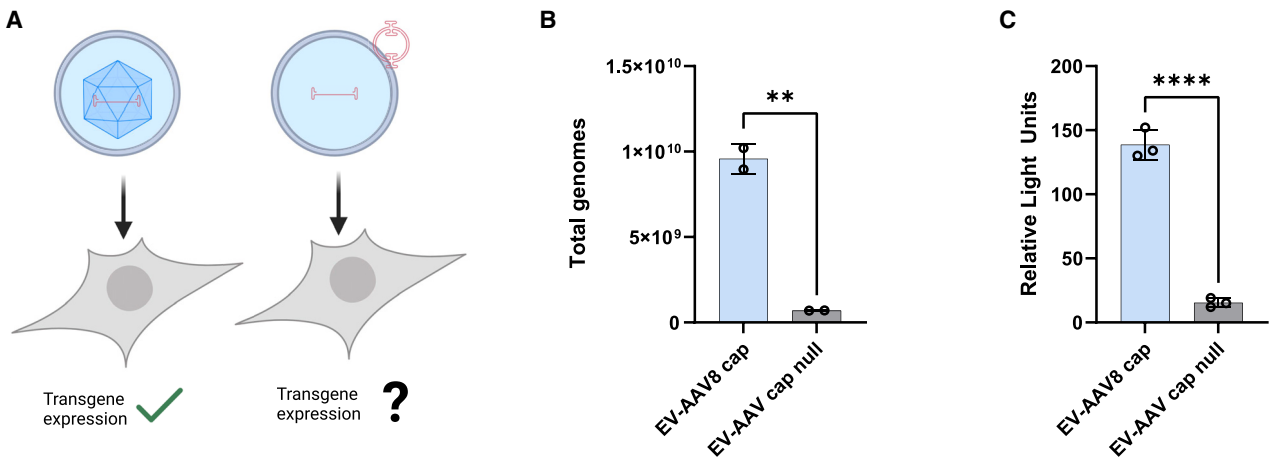

Figure 5. The AAV capsid is required for efficient transduction by EV-AAV

(A) HeLa cells were transduced by either EV-AAV8-FLuc vector (gradient fractions 1–6) or EVs isolated from fractions 1–6, which were isolated from 293T cells transfected with AAV-FLuc plasmid but no AAV8 rep/cap plasmid. (B) Total AAV vector genomes isolated from gradient fractions 1–6 for either preparation. $^{**}p = 0.005$. (C) Transduction efficiency on HeLa cells incubated with 6.66×10^3 vg/cell of either preparation. $^{****}p < 0.0001$.

should theoretically be competent at transduction. However, since we and others have observed AAV capsids on the surface and interior of EVs, either location could plausibly lead to transduction upon uptake into cells. To assess whether luminal EV-AAV was (a) present at detectable quantities in EV-AAV preparations and (b) if it could mediate transduction and evade antibody neutralization, we removed EVs containing an external AAV capsid using anti-AAV9 conjugated magnetic beads. We found that approximately 11% of purified EV-AAV9 were protected from pulldown, demonstrating a significant portion is luminal. This is an underestimate of all luminal EV-AAV, as EVs that contained both AAV9 capsid on the surface and interior would be pulled down and not quantitated. In future research, the removal of non-covalently bound AAV from the EV surface may be achieved through specific buffer treatments which contain high salt or pH optimization. This could increase the yield of solely luminal EV-AAV vectors. We observed that anti-AAV9 pulldown-resistant vectors mediated robust transduction of cultured cells as well as resistance to antibody neutralization. We also compared standard AAV9, EV-AAV9, and intraluminal EV-AAV9 for transduction after intracranial injection into the striatum of adult mice. Intraluminal EV-AAV9 mediated transduction of neurons. However, EV-AAV9, which contains both surface-bound and intraluminal EV-AAV9, showed the most robust transduction in the brain, greatly surpassing the other two groups, which included standard AAV9. This was quite remarkable given the small dose of AAV used in this experiment (approximately 10^7 vg into the striatum). Another study showed increased spread and stability of EV-AAV6 and EV-AAV9 transduction compared with standard AAV after intracranial injection.[18] This suggests that EV-AAV9 may be useful when local, but widespread transduction of the brain is desired, such as for large structures like the striatum, especially in larger brains. While intraluminal EV-AAV transduction efficiency was less than EV-AAV, the former may be more desirable in the presence of anti-AAV antibodies, which can also be present in brain.[25] A recent report demonstrated that AAV can be re-dosed in brain in the presence of low antibodies by limiting the initial intracranial dose.[26] This holds great promise for EV-AAV re-dosing in the brain, which is much more resistant than standard AAV, and may expand the dose range that can be used. In future research we will explore EV-AAV spread in large brains (e.g., non-human primates) as well as in the presence of neutralizing antibodies.

Current yields of EV-AAV, as evidenced in Figure 1, are much lower than conventional, free AAV. To attempt to improve EV-AAV yields we used *trans*-expression of MAAP8, which was previously demonstrated to increase AAV export to the cell culture media.[24] Interestingly, we found that MAAP8 co-transfected with an AAV9 cap/MAAP-null plasmid yielded 3-fold higher vector genomes than a conventional AAV9 system. Free AAV yields were also increased by this approach, which suggests that MAAP8, at least in the conditions tested with AAV9, does not selectively increase AAV interactions with EVs. We also tested *trans*-expression of AAV9 MAAP9. In this experiment we used a pcDNA plasmid with a strong CMV promoter driving either MAAP8 or MAAP9. We observed apparent toxicity of MAAP overexpression at the highest DNA amount tested (data not shown). At a lower amount of MAAP9 plasmid we observed a 2-fold increase in EV-AAV yield compared with the cis MAAP9 system (Figure S5). In contrast, the pcDNA-CMV-MAAP8 plasmid did not increase EV-AAV amounts over cis MAAP9 system. This is in sharp contrast to the increase in EV-AAV yield observed when MAAP8 was expressed in trans under the AAV p40 promoter. The apparent discrepancy is likely due to the weaker p41 promoter vs. the strong CMV promoter which may have led to toxicity in the latter case. Further evidence in that MAAP9 is more weakly expressed than MAAP8, which may explain the results in the pcDNA-CMV-MAAP experiment with MAAP9 increasing EV-AAV yields compared with

MAAP8 (personal correspondence with Asokan lab). Interestingly AAV6, showed the higher ratio of EV-AAV:free AAV of the serotypes tested (Figure S1). It may be worthwhile to test *trans*-expression of AAV6 MAAP to increase yields of EV-AAV in other serotypes, although it is possible other AAV6 proteins, including VP1, 2, and 3, are involved in the greater EV-AAV association. In the future, combining approaches that selectively incorporate AAV into EVs along with MAAP overexpression may yield higher EV-AAV yields, as well as lower percentages of free AAV in the media.

The purpose of this study was to increase the characterization of the EV-AAV system to improve it in future research. To do this, we used the relatively non-scalable approach of density gradient ultracentrifugation, as it is an established and productive method to achieve high purity and separation of biomolecules including EVs and AAV vectors. In terms of scaling the system up for manufacturing of larger batches of EV-AAV, that was outside the scope of this study. However, some of our findings may be relevant to the manufacturing and downstream processing of EV-AAV. For example, careful titration of MAAP expression as mentioned above should help to increase yields of EV-AAV. Second, our observation that luminally localized AAV capsids in EVs can mediate enhanced transduction and antibody evasion should drive research efforts toward improved packaging of AAV into EVs, as well as downstream steps to remove free AAV. While we demonstrated the pulldown of free AAV capsids from EV-AAV preparations using a "batch" method, this could be done at industrial scale using chromatography columns bounds with anti-AAV resins that are already commercially available. It should be mentioned that a recent study used industry-compatible scale-up to produce EV-AAV. Chen et al.[27] used suspension cells in stirred tank bioreactors to produce EV-AAV and purified them using size exclusion chromatography. In future research, we will combine our knowledge from our current study with these scalable methods to produce higher yields of EV-AAV.

As mentioned earlier, the AAV capsid performs all functions of delivery of the AAV genome to the recipient cell; thus, it is indispensable for robust AAV transduction. In contrast, since EVs are themselves capable of biomolecule delivery, capsid-free AAV genomes or residual plasmid DNA could mediate transgene expression if sufficient DNA was delivered to the nucleus. Thus, we tested whether a capsid-less EV-AAV genome system could mediate similar levels of transgene expression observed with the capsid containing EV-AAV system. We used a sensitive luciferase transgene expression cassette so that we could detect even low levels of transduction. We did in fact detect very low levels of transduction (approximately 2-fold over background levels) with the capsid-less EV-AAV preparation. This level of activity may have been caused by residual plasmid DNA, mRNA, or AAV genomes. It is unlikely to be caused by luciferase protein in the preparation, as FLuc has a short half-life of approximately 3 h. In contrast, the luciferase activity was 9-fold higher in EV-AAV8-FLuc vectors. These data suggest that the capsid is an essential component of the EV-AAV delivery system. Post cellular uptake of EV-AAV, the capsid is likely responsible for intracellular transport of the genome into the nucleus, similar to conventional AAV.

In all, our work described here increases our understanding of the EV-AAV delivery system, which can be leveraged for further development of the platform.

MATERIALS AND METHODS

Cell culture

Human 293T or HeLa cells were obtained from American Type Culture Collection (Manassas, VA). Cells were cultured in high glucose DMEM HEPES (Invitrogen, Carlsbad, CA) supplemented with 10% fetal bovine serum (FBS) (Sigma, St. Louis, MO) and 1× Gibco penicillin-streptomycin-glutamine (100 U/mL penicillin, 100 μg/mL streptomycin, 292 μg/mL L-glutamine (Invitrogen) in a humidified atmosphere supplemented with 5% CO_2 at 37°C.

Animals

All animal experiments were approved by the Massachusetts General Hospital Subcommittee on Research Animal Care following guidelines set forth by the National Institutes of Health Guide for the Care and Use of Laboratory Animals. We used adult age (8–10 weeks old) female C57BL/6 (strain # 000664) from The Jackson Laboratory (Bar Harbor, ME).

AAV and EV-AAV vector production

For each production, we plated 15-cm tissue culture dishes with 1.5×10^7 293T cells/dish. The next day cells were triple-plasmid transfected using polyethyleneimine (PEI) method, with the adenovirus helper plasmid (pAdΔF6, 15 μg per plate), *rep/cap* plasmid (pAR9 for AAV9, 7 μg per plate), and inverted terminal repeat (ITR)-flanked AAV transgene expression cassette (either single-stranded AAV-CBA-GFP or AAV-CBA-Fluc, 6 μg/plate, encoding green fluorescent protein or FLuc, respectively) to induce production of AAV. The day after transfection, medium was changed to DMEM containing 2% FBS (bovine EV-depleted FBS). Three days post transfection, cell lysates (standard AAV) or cell culture media (EV-AAV) were harvested for further processing as described below.

Iodixanol gradient purification of EV-AAV

The cell culture media for purified EV-AAV was processed identically to the pelleted exo-AAV method up to and including the 20,000×*g* large vesicle depletion step. Media was treated with Benzonase (25 U/mL with 2 mM $MgCl_2$) for 1 h at 37°C. Next, the media was concentrated using Amicon Ultra-15 100kDa centrifugal filters. A gradient consisting of 5mL of 15% iodixanol, 10 mL of 25% iodixanol, 3 mL of 40%, and 2 mL of 60% iodixanol was created by hand using an underlay method. Twenty milliliters of concentrated, Benzonase-treated producer cell media was loaded on top of the gradient which was loaded into a 70Ti rotor (Beckman Coulter, Brea, CA) and ultracentrifuged in an Optima XE-90 Ultracentrifuge (Beckman Coulter) at 250,000×*g* for 3 h at 4°C. At the end of the run, the rotor coasted to a stop with no brake. To isolate purified EV-AAV, we removed the approximately 14%–20% fraction (putative

EV-containing fraction) corresponding to 10 mL of volume. In some experiments we also collected the 40%–60% layers containing free AAV. Next, the EV-AAV containing fraction was subjected to buffer exchange (to PBS) and concentration using an Amicon Ultra 100-kDa molecular weight cutoff centrifugal device. Purified EV-AAV was pipetted into single-use aliquots and stored at −80°C until use.

Iodixanol gradient purification of conventional AAV

AAV was purified from the freeze/thawed cell lysate using iodixanol density-gradient ultracentrifugation. Buffer exchange to PBS/0.001% Pluronic F68 was done using ZEBA spin columns (7K MWCO; Thermo Fisher Scientific, Waltham, MA) and further concentration was performed using Amicon Ultra 100k Da MWCO ultrafiltration centrifugal devices (Millipore, Burlington, MA). Vectors were stored at −80°C until use.

qPCR titration of AAV genomes

Before titration, EV-AAV and AAV samples were treated with DNase I to remove plasmid DNA from the transfection by mixing 5 μL of the sample with 1 μL DNase I, 5 μL 10× buffer, and 39 μL water. Samples were incubated 1 h at 37°C and then DNase I was inactivated at 75°C for 15 min. We purified AAV genomes using High Pure Viral Nucleic Acid Kit (Roche, Indianapolis, IN) according to the manufacturer's protocol. Next, vector genome samples were titered (expressed as vector genomes/ml) using a quantitative TaqMan PCR that detects AAV genomes (polyA region of the transgene cassette) in a 7500 Fast Real-Time PCR system (Applied Biosystems, Foster City, CA) as previously described.[28]

ExoView quantitation of tetraspanin-positive EVs

To quantitate EV quantity, tetraspanin marker expression, and size we used the ExoView R100 instrument in conjunction with the ExoView Tetraspanin Kit (NanoView Biosciences, Brighton, MA). In brief, this instrument consists of a fluorescence and interferometric microscope which detects single EVs captured on chips coated with antibodies specific to tetraspanin proteins expressed on EVs. The instrument can size EVs (range, 50–200 nm) and also quantitate numbers of EVs by detecting fluorescence from bound labeled antibodies. Fractions from size exclusion chromatography were diluted 1:400 and incubated 16 h at room temperature on tetraspanin chips printed with antibodies against CD81, CD63, CD9, or an isotype control antibody. The following day, the chips were rinsed four times with rapid shaking on an orbital shaker. Next, fluorescently labeled secondary antibodies specific for CD9, CD63, and CD81 were added to the chip and incubated for 1 h. After extensive washing, chips were dried and then inserted into the ExoView instrument for scanning and data acquisition. Data were analyzed using the ExoView Analyzer software.

Anti-capsid immunoblots

Samples from gradient purified EV-AAV, were loaded onto an 4–12% SDS PAGE Bis-Tris gel (Thermo Fisher Scientific) and electrophoresed for 1.5 h at 120 V. Proteins were transferred to nitrocellulose membrane for 1 h at 30 V. For the detection of AAV capsid proteins VP1, VP2, and VP3, rabbit polyclonal antibody to AAV capsid was used (product #03–61084, American Research Products, Waltham, MA). A secondary horse radish peroxidase-conjugated anti-rabbit antibody (catalog # NA934VS, Cytiva, Marlborough, MA) was used for detection of capsid. Chemiluminescence was detected with SuperSignal West Femto Maximum Sensitivity Substrate (Thermo Fisher Scientific) and membranes exposed to Hyblot CL autoradiography film (Lab Force, Thomas Scientific, Swedesboro, NJ).

Cryo-EM

Cryo-EM of pooled fractions 1–6 of the iodixanol gradients ultracentrifuged with media from AAV producing 293T cells was performed at the University of Massachusetts Chan Medical School Cryo-EM Core facility as previously described.[12]

Anti-AAV capsid pulldown

CaptureSelect Biotin anti-AAV9 conjugate (cat. No. 7103332100, Thermo Fisher Scientific) or CaptureSelect Biotin Anti-AAVX Conjugate (Catalog number: 7103522100 Thermo Fisher Scientific) was bound to Dynabeads Streptavidin beads M-280 (11205D, Thermo Fisher Scientific) for 30 min at room temperature (RT) on a tube rotator. After magnet binding of complexed antibody:beads, beads were washed. Next, 10^{10} vg of AAV9 or EV-AAV9 (for anti-AAV9 conjugate) or AAV1, AAV2, AAV6, AAV9, or their EV counterparts (for anti-AAVX conjugate) were added to the beads and incubated for 1 h at RT on a tube rotator. The solution was placed on a magnet for 2 min to pulldown the AAV:antibody:bead complex and the supernatant was collected for AAV genome titration by qPCR. We calculated the percent of AAV vector resistance to pulldown using the following formula: Total vector genomes in supernatant after pulldown/Total input vector genomes × 100.

HeLa transduction and IVIg neutralization assay

In vitro neutralization assays were performed with Gamunex-C purified IVIg (Grifols, Barcelona, Spain) or with pooled normal human sera (Innovative Research, Novi, MI). HeLa cells were seeded at 10,000 cells per well in a 96-well plate the day before the assay. Next, a dose of 1×10^4 vg/cell of AAV9-FLuc or EV-AAV9-Fluc was mixed with serial dilutions of IVIg in FBS-free media. Vector samples mixed with media served as control. These were incubated for 1 h at 37°C before adding to cells for 1.5 h at 37°C. After washing cells one time, and replacing with complete medium, cells were incubated for 48 h before performing a luciferase assay using Bright-Glo Luciferase reagent (Promega, Madison, WI). A BioTek Synergy HTX multi-mode luminometer (BioTex, Winooski, VT) was used to detect luminescence. Luciferase values for each sample, expressed in relative light units were plotted as a fraction of the AAV transduction sample without serum (which was set to 1.0).

MAAP transfection experiments

We produced EV-AAV for the MAAP trans complementation in a similar manner to that described above with the following modifications. The AAV9 MAAP null plasmid (pLH9-MAAP null) rep/cap expresses AAV9 capsid proteins, but not AAV9 MAAP.[24] The

AAV8-MAAP8 plasmid (pLH8-VP null), rep/cap expresses MAAP8 under the endogenous p40 promoter but not AAV8 capsid proteins due to an intentional mutated start codon.[24] We performed a PEI transfection of 293T cells with the following plasmids/DNA per 15-cm cell culture dish: (1) pAAV-CAG-GFP ITR flanked expression cassette (5.6 μg), (2) pAdΔF6 (adenovirus helper plasmid, 12 μg), (3) pAR9 (AAV9 rep/cap, 5 μg) or pLH9-MAAP null (5 μg), and (4) pLH8-VP Null or salmon sperm DNA 5.0 μg. Media was changed the day after transfection to EV-depleted FBS containing media and at the desired time point, media was harvested for iodixanol gradient EV-AAV purification.

VP-null transfection experiment

We transfected 293T cells with (1) pAAV-CBA-FLuc ITR-flanked expression cassette (6 μg), (2) pAdΔF6 (adenovirus helper plasmid, 15 μg), or (3) AAV8 rep/cap (5 μg) or pLH8-VP null (expresses, rep, MAAP, but no capsid; 5 μg). Media was changed the day after transfection to EV-depleted FBS containing media and at day 3 after transfection, media harvested for iodixanol gradient EV-AAV purification. For both EV-AAV8 and EV-AAV VP null transfected cells, we harvested fractions 1–6 from the gradient for use in titering assays as well as transduction of HeLa cells.

Intracranial injection of AAV vectors

Adult C57BL/6 mice (n = 3/group) were injected stereotactically into the striatum with 1.27×10^7 vg of each vector preparation (AAV9, EV-AAV9, IL-EV-AAV9, all packaging AAV-CAG-GFP) in a volume of 3 μL. Mice were placed into a *Just For Mouse* Stereotaxic Frame (Stoelting, Wood Dale, IL). AAV vectors were infused in the left midstriatum using the following coordinates from bregma in mm: AP +0.5, ML +2.0, DV −2.5. AAV vectors were infused into the striatum at a rate of 0.2 μL/min using a Quintessential Stereotactic Injector pump (Stoelting) to drive a gas-tight 10 μl NEUROS model Hamilton Syringe (Hamilton, NV) attached to a 33-gauge needle (Hamilton).

Brain tissue processing and immunofluorescence imaging

Intracranially injected animals were euthanized 4 weeks after injection, perfused transcardially with 4% formaldehyde in PBS. Brains were post-fixed in 4% formaldehyde diluted in PBS for 48 h, followed by 30% sucrose for cryopreservation for another 48–72 h after which brains were embedded and frozen in Tissue-Tek O.C.T. compound (Sakura Finetek USA, Torrance, CA). Coronal floating sections (40 μm) were cut using an NX50 CryoStar Cryostat (Thermo Fisher Scientific). Fluorescence imaging of whole brain coronal sections was performed using a KEYENCE BZ-X800 microscope (KEYENCE Corporation of America, Itasca, IL). A 4× overview of each slide was taken before scanned 10× images of the coronal brain section with a 2.5-s exposure for fluorescence detection were acquired. Images were automatically stitched using BZ-X100 Analyzer Software (KEYENCE).

Quantitation of transduced area for each vector

To quantitate the area of striatum transduced by each vector, we used FIJI (FIJI is just ImageJ) software version 1.54f[29] using the "Analyze" >"Measure" function. We used Integrated Density to quantitate transduction as it measures the product of the transduced area × the pixel intensity. To do this we analyzed transduction at or near the injection site for representative section for each mouse for each vector group. Fluorescence images were converted to 8-bit grayscale images and thresholded to remove non-bright signals. Next, a region of interest (ROI) was drawn around the area of transduction using the polygon ROI tool. This was performed for each section of interest.

Statistics

We used GraphPad Prism 9.0 for PC for statistical analysis. For comparison of multiple groups, we used either a one-way or two-way ANOVA (depending on the number of independent variables) followed by a Tukey's multiple comparisons test. For comparison of two groups, we used a two-sided unpaired Student t test. A p value of less than 0.05 was considered statistically significant.

DATA AND CODE AVAILABILITY

Data are available upon request.

ACKNOWLEDGMENTS

BioRender software was used for generation of the artwork in the figures. C.A.M. discloses support from the research described in this study from the NIH [grant# DC017117]. We thank Gang Fu and KangKang Song of the UMass Chan Medical School Cryo-EM Core Facility for performing Cryo-EM on the EV-AAV sample as well as assistance in image analysis. We thank the Molecular Imaging Center MGH Campus Navy Yard (CNY) for the use of the confocal microscope.

AUTHOR CONTRIBUTIONS

C.A.M. conceived of and designed the study. D.D.L.C., A.V.C., P.E., and M.C. performed experiments and analyzed data. A.A. and Z.E. helped design experiments and analyze data. C.N. performed experiments. C.A.M., D.D.L.C., and M.C. wrote the manuscript with contributions and/or revisions from all authors.

DECLARATION OF INTERESTS

C.A.M. has financial interests in Chameleon Biosciences, Skylark Bio, and Sphere Gene Therapeutics, companies developing adeno-associated virus (AAV) vector technologies for gene therapy applications. C.A.M. performs paid consulting work for all three companies. C.A.M. has pending and issued patents surrounding EV-AAV technology, which has been licensed to biotechnology companies. C.A.M.'s interests were reviewed and are managed by Massachusetts General Hospital and Mass General Brigham in accordance with their conflict-of-interest policies.

SUPPLEMENTAL INFORMATION

Supplemental information can be found online at https://doi.org/10.1016/j.omtm.2025.101407.

REFERENCES

1. Ghauri, M.S., and Ou, L. (2023). AAV Engineering for Improving Tropism to the Central Nervous System. Biology *12*, 186.

2. Berry, G.E., and Asokan, A. (2016). Cellular transduction mechanisms of adeno-associated viral vectors. Curr. Opin. Virol. *21*, 54–60.

3. Loeb, E.J., Havlik, P.L., Elmore, Z.C., Rosales, A., Fergione, S.M., Gonzalez, T.J., Smith, T.J., Benkert, A.R., Fiflis, D.N., and Asokan, A. (2024). Capsid-mediated control of adeno-associated viral transcription determines host range. Cell Rep. *43*, 113902.

4. Manno, C.S., Pierce, G.F., Arruda, V.R., Glader, B., Ragni, M., Rasko, J.J., Ozelo, M.C., Hoots, K., Blatt, P., Konkle, B., et al. (2006). Successful transduction of liver in

hemophilia by AAV-Factor IX and limitations imposed by the host immune response. Nat. Med. *12*, 342–347.

5. Mingozzi, F., and High, K.A. (2013). Immune responses to AAV vectors: overcoming barriers to successful gene therapy. Blood *122*, 23–36.
6. Salabarria, S.M., Corti, M., Coleman, K.E., Wichman, M.B., Berthy, J.A., D'Souza, P., Tifft, C.J., Herzog, R.W., Elder, M.E., Shoemaker, L.R., et al. (2024). Thrombotic microangiopathy following systemic AAV administration is dependent on anti-capsid antibodies. J. Clin. Invest. *134*, e173510.
7. (2020). High-dose AAV gene therapy deaths. Nat. Biotechnol. *38*, 910.
8. Guillou, J., de Pellegars, A., Porcheret, F., Frémeaux-Bacchi, V., Allain-Launay, E., Debord, C., Denis, M., Péréon, Y., Barnérias, C., Desguerre, I., et al. (2022). Fatal thrombotic microangiopathy case following adeno-associated viral SMN gene therapy. Blood Adv. *6*, 4266–4270.
9. Lek, A., Wong, B., Keeler, A., Blackwood, M., Ma, K., Huang, S., Sylvia, K., Batista, A.R., Artinian, R., Kokoski, D., et al. (2023). Unexpected Death of a Duchenne Muscular Dystrophy Patient in an N-of-1 Trial of rAAV9-delivered CRISPR-transactivator. Preprint at medRxiv. https://doi.org/10.1101/2023.05.16.23289881.
10. Morales, L., Gambhir, Y., Bennett, J., and Stedman, H.H. (2020). Broader Implications of Progressive Liver Dysfunction and Lethal Sepsis in Two Boys following Systemic High-Dose AAV. Mol. Ther. *28*, 1753–1755.
11. Maguire, C.A., Balaj, L., Sivaraman, S., Crommentuijn, M.H.W., Ericsson, M., Mincheva-Nilsson, L., Baranov, V., Gianni, D., Tannous, B.A., Sena-Esteves, M., et al. (2012). Microvesicle-associated AAV vector as a novel gene delivery system. Mol. Ther. *20*, 960–971.
12. Cheng, M., Dietz, L., Gong, Y., Eichler, F., Nammour, J., Ng, C., Grimm, D., and Maguire, C.A. (2021). Neutralizing Antibody Evasion and Transduction with Purified Extracellular Vesicle-Enveloped Adeno-Associated Virus Vectors. Hum. Gene Ther. *32*, 1457–1470.
13. Gyorgy, B., Fitzpatrick, Z., Crommentuijn, M.H., Mu, D., and Maguire, C.A. (2014). Naturally enveloped AAV vectors for shielding neutralizing antibodies and robust gene delivery in vivo. Biomaterials *35*, 7598–7609.
14. Gyorgy, B., Sage, C., Indzhykulian, A.A., Scheffer, D.I., Brisson, A.R., Tan, S., Wu, X., Volak, A., Mu, D., Tamvakologos, P.I., et al. (2017). Rescue of Hearing by Gene Delivery to Inner-Ear Hair Cells Using Exosome-Associated AAV. Mol. Ther. *25*, 379–391.
15. Hudry, E., Martin, C., Gandhi, S., György, B., Scheffer, D.I., Mu, D., Merkel, S.F., Mingozzi, F., Fitzpatrick, Z., Dimant, H., et al. (2016). Exosome-associated AAV vector as a robust and convenient neuroscience tool. Gene Ther. *23*, 380–392.
16. Meliani, A., Boisgerault, F., Fitzpatrick, Z., Marmier, S., Leborgne, C., Collaud, F., Simon Sola, M., Charles, S., Ronzitti, G., Vignaud, A., et al. (2017). Enhanced liver gene transfer and evasion of preexisting humoral immunity with exosome-enveloped AAV vectors. Blood Adv. *1*, 2019–2031.
17. Wassmer, S., Carvalho, L., Gyorgy, B., Vandenberghe, L.H., and Maguire, C.A. (2017). Exosome-Associated AAV2 vector mediates robust gene delivery into the murine retina upon intravitreal injection. Sci. Rep. *7*, 45329.
18. Orefice, N.S., Souchet, B., Braudeau, J., Alves, S., Piguet, F., Collaud, F., Ronzitti, G., Tada, S., Hantraye, P., Mingozzi, F., et al. (2019). Real-Time Monitoring of Exosome Enveloped-AAV Spreading by Endomicroscopy Approach: A New Tool for Gene Delivery in the Brain. Mol. Ther. Methods Clin. Dev. *14*, 237–251.
19. Li, X., La Salvia, S., Liang, Y., Adamiak, M., Kohlbrenner, E., Jeong, D., Chepurko, E., Ceholski, D., Lopez-Gordo, E., Yoon, S., et al. (2023). Extracellular Vesicle-Encapsulated Adeno-Associated Viruses for Therapeutic Gene Delivery to the Heart. Circulation *148*, 405–425.
20. Schiller, L.T., Lemus-Diaz, N., Rinaldi Ferreira, R., Böker, K.O., and Gruber, J. (2018). Enhanced Production of Exosome-Associated AAV by Overexpression of the Tetraspanin CD9. Mol. Ther. Methods Clin. Dev. *9*, 278–287.
21. Liu, B., Li, Z., Huang, S., Yan, B., He, S., Chen, F., and Liang, Y. (2021). AAV-Containing Exosomes as a Novel Vector for Improved Gene Delivery to Lung Cancer Cells. Front. Cell Dev. Biol. *9*, 707607.
22. Florea, M., Nicolaou, F., Pacouret, S., Zinn, E.M., Sanmiguel, J., Andres-Mateos, E., Unzu, C., Wagers, A.J., and Vandenberghe, L.H. (2023). High-efficiency purification of divergent AAV serotypes using AAVX affinity chromatography. Mol. Ther. Methods Clin. Dev. *28*, 146–159.
23. Ogden, P.J., Kelsic, E.D., Sinai, S., and Church, G.M. (2019). Comprehensive AAV capsid fitness landscape reveals a viral gene and enables machine-guided design. Science *366*, 1139–1143.
24. Elmore, Z.C., Patrick Havlik, L., Oh, D.K., Anderson, L., Daaboul, G., Devlin, G.W., Vincent, H.A., and Asokan, A. (2021). The membrane associated accessory protein is an adeno-associated viral egress factor. Nat. Commun. *12*, 6239.
25. Treleaven, C.M., Tamsett, T.J., Bu, J., Fidler, J.A., Sardi, S.P., Hurlbut, G.D., Woodworth, L.A., Cheng, S.H., Passini, M.A., Shihabuddin, L.S., and Dodge, J.C. (2012). Gene transfer to the CNS is efficacious in immune-primed mice harboring physiologically relevant titers of anti-AAV antibodies. Mol. Ther. *20*, 1713–1723.
26. Xu, Y., Bai, X., Lin, J., Lu, K., Weng, S., Wu, Y., Liu, S., Li, H., Chen, G., and Li, W. (2024). Antibodies against the capsid induced after intracranial AAV administration limits second administration in a dose dependent manner. Preprint at bioRxiv. https://doi.org/10.1101/2024.09.15.612566.
27. Chen, K., Ernst, P., Sarkar, A., Kim, S., Si, Y., Varadkar, T., Ringel, M.D., Liu, X., and Zhou, L. (2024). mLumiOpto is a Mitochondrial-Targeted Gene Therapy for Treating Cancer. Cancer Res. *84*, 4049–4065.
28. Bennett, J., Ashtari, M., Wellman, J., Marshall, K.A., Cyckowski, L.L., Chung, D.C., McCague, S., Pierce, E.A., Chen, Y., Bennicelli, J.L., et al. (2012). AAV2 gene therapy readministration in three adults with congenital blindness. Sci. Transl. Med. *4*, 120ra15.
29. Schindelin, J., Arganda-Carreras, I., Frise, E., Kaynig, V., Longair, M., Pietzsch, T., Preibisch, S., Rueden, C., Saalfeld, S., Schmid, B., et al. (2012). Fiji: an open-source platform for biological-image analysis. Nat. Methods *9*, 676–682.